https://doi.org/10.48048/tis.2023.3566

Theoretical and Experimental Approach for the Sensation of Urine Ubiquitin Conjugating Enzyme E2 C (UBE2C) mRNA Related to Bladder Cancer by Polyacrylamide Sensor Doped with Zinc Oxide

Noha Asker[1] and Raghda Abou Gabal[2,*]

[1]Department of Basic Science, Faculty of Engineering, Horus University, Damietta, Egypt
[2]Mansoura Urology and Nephrology Center, Mansoura University, Dakahlia Governorate, Egypt

([*]Corresponding author's e-mail: raghdaabogabal@gmail.com)

Received: 5 April 2022, Revised: 16 May 2022, Accepted: 23 May 2022, Published: 30 November 2022

Abstract

Bladder cancer (BC) is the ninth and 4 most prevalent cancer in men worldwide and in the United States. Urothelial carcinoma (UC) is the most common histological kind. Biosensors are devices that translate complex biological events into an electrical signal whose intensity is proportional to the analyte's concentration, allowing them to detect a specific biological analyte. The nanotechnology with nanoparticles improves and modifies the biorecognition element to improve the biosensing phenomenon, making it one of the most popular subjects among scientists. Employment of ZincOxide (ZnO) nanoparticles into the polyacrylamide (PAM) is supposed to enhance electrical and sensory capabilities that promise more inventive and faster detection with improved repeatability.

Studying the ability of PAM\ZnO nanocomposite to sense Urine Ubiquitin Conjugating Enzyme E2 C (UBE2C), the nanocomposite's interactions with the enzyme was studied using a modeling model, and then the PAM\ZnO nanocomposite was prepared and studied with spectroscopic technique. Consequently, the Fourier Transform Infrared (FTIR) spectra for PAM\ZnO resulted in peaks in the 400 - 600 cm^{-1} range that vanished in acidic media.

Density functional theory (DFT) calculations were performed at B3LYPL using the basis set 6-31G on PAM\ZnO nanocomposites with cysteine 114. The findings of the HOMO/LUMO bandgap energy, total dipole moment (TDM), and Molecular Electrostatic Potential (MESP) indicated that the effect of ZnO in the presence of PAM gives a nanocomposite with high electronic characteristics with a TDM ranging from 5.4464 to 12.3348 Debye, and bandgap (ΔE) 0.19965 to 0.28302 eV. A variation in the electrostatic characteristics of this composite followed the addition of Cystine 114. The distinctive properties of such nanocomposite PAM/ZnO enable usage in biosensor applications for bladder cancer. Finally, the FTIR spectrum showed that the estimated model fits as a proper biosensor.

Keywords: Biosensor, Bladder cancer, Modeling, FTIR, Polyacrylamide, ZnO nanoparticle, Cysteine 114, UBE2C

Introduction

Bladder cancer (BC) is one of the deadliest cancers globally. Muscle-invasive (MIBC) and muscle-non-invasive (NMIBC) BC are 2 types. (NMIBC) BC recur frequently and advance to MIBCs, which have a lower survival rate and a higher rate of distant metastasis. Computed Tomography (CT), which uses X-rays to give cross-sectional imaging, is the most frequent imaging modality used to monitor. Magnetic Resonance Imaging (MRI) is a technique for detecting abnormalities that uses powerful magnetic fields. Ultrasound evaluation of the cervix, pancreas, liver, and kidneys is always beneficia [1,2]. The most well-known issue with these diagnostic procedures is the significant possibility of false positives.

Tissue biopsy is a standard method for diagnosing and investigating cancer. Nonetheless, obtaining tissue from a single solitary tumor may not provide complete information about the patient's state. On the other hand, multiple tissue extractions are not recommended to overcome cancer heterogeneity because each extraction increases the chance of disease diffusion to other body sections. Furthermore, the placement of some tumors renders sample extraction extremely difficult or impossible [3-5]. Because tissue biopsy has limits, a liquid biopsy was developed to detect cancer biomarkers in body fluids such as blood, serum, saliva, and urine to aid cancer screening, diagnosis, and therapy. A liquid biopsy is less invasive and more robust against disease heterogeneity [5].

A growing body of data shows that "Liquid biopsy" can identify urine biomarkers like circulating cell-free DNA, DNA methylation, miRNA, cell-free proteins/peptides, and exosomes [6,7]. These biomarkers must be able to be used in clinical applications. Innovative analytical methods must identify them at low concentrations in complex sample matrices. In the management of BC, nanotechnology has been proposed as an innovative system. Nanotechnology can be combined with other cutting-edge technologies (such as phototherapy and radiotherapy) to boost efficacy further. More effective and accurate ways of detecting and treating BC are predicted to emerge as nanotechnology and ontogenetic mechanisms evolve.

Because of their unique optoelectronic characteristics and ease of functionalization, metal nanoparticles have emerged as exceptional analytical scaffolds. As a result, various analytical approaches based on these nanoparticles and their plasmonic capabilities have been developed. Various methodologies and technologies for measuring biomarkers have been described, including biosensors that need bioreceptor usage. This unique property of gold nanoparticle (AuNPs) was used by Nossier *et al.* [8] to detect hyaluronidase in the urine of bladder cancer patients directly. Formation of gold aggregates with red to blue color shift indicated the presence of hyaluronidase. Eissa *et al.* [9] developed an AuNP assay for BC diagnosis to directly detect unamplified hepatoma upregulated RNA (HURP RNA). Zou *et al.* [10] created AuNPs-based devices to monitor telomerase activity. However, large-scale synthesis of AuNPs for clinical use may be complex, and the established test may be expensive, preventing AuNPs from being used in the clinic. On a practical level, cost-effectiveness is critical. Patel *et al.* developed a biosensor using amorphous Ge2Sb2Te5 (GST) in various design structures, which they tested on various quantities of biomolecules such as hemoglobin and urine [11]. The role of zinc oxide nanoparticles in the selective killing of tumor cells was demonstrated by Rasmussen *et al.* [12] Active sites made of ZnO nanostructures have a lot of biosensor potential. The morphologies of ZnO nanostructures have huge surface areas.

Ogiso *et al.* [14] was combined MIP (molecularly imprinted polymers) technology with gel electrophoresis to create a simple and inexpensive DNA detection tool. MIPs are synthetic materials utilized as recognition elements in sensor design because of their superior thermal stability, reusability, and selectivity over biological receptors [13,14]. In the presence of a template, MIP is made by polymerizing functional monomers and cross-linker molecules. The cavities can engage selectively with the target molecule in a complex sample. The variation of a physical attribute is the result of this interaction. Some protein biomarkers, such as bovine (and human) serum albumin, hemoglobin, myoglobin (Mb), and prostate-specific antigen, have been determined using MIP-based biosensor [15,16]. Wang *et al*. was studied Polyacrylamide hydrogel as a molecularly imprinted polymer. The backbone of gel electrophoresis is polyacrylamide (PAM). Water-soluble monomers like acrylamide and functionalized acrylamides have been combined with the cross-linker N, N′-methylenebisacrylamide (MBAM) to create polyacrylamide-based MIPs for hydrogel protein imprinting [16]. Polyacrylamide (PAM) is biocompatible and resistant to nearly all non-specific protein interactions.

Commercially available urine-based assays for BC detection and surveillance have been approved by the Food and Drug Administration (FDA). Because of the amount of cell-free nucleic acid in the supernatant or sediments, the urine appears to be a good source for miRNA identification [6]. Urine Ubiquitin Conjugating Enzyme E2 C (UBE2C) mRNA is circulating messenger RNAs (mRNAs); UBE2C (ubiquitin-conjugating enzyme E2C) expression has been linked to high tumor grade and cancer progression in BC. It is crucial for mitotic destruction events [17,18].

This paper proposes computational modeling research for the development of UBE2C biosensors. Computational tools such as hit detection, lead optimization, and structure-based virtual screening have become essential components of many drug development programs. Virtual screening is a method of searching small chemical libraries for a specific subset of compounds that interact with a therapeutic protein target. Understanding UBE2C's 3D structure will help researchers better understand its function and role in cells, analyze its molecular interactions with other proteins, and develop new inhibitors. The homology modeling was discovered using the NCBI BLAST program. Human Mitotic-Specific Ubiquitin Conjugating Enzyme Crystal Structure (PDB code: 117K).

This study aims to see how decorating with zinc oxide ZnO affects polyacrylamide PAM utilizing B3LYP/3-21g. The experimental results of ZnO/PAM preparation and FTIR characterization are compared to the researched model.

Materials and methods

Materials

As a monofunctional monomer (cross-linker), acrylamide ($C_2H_3CONH_2$) was utilized, and as a difunctional monomer (cross-linker), N, N′-methylene bisacrylamide ((C2H3CONH2)2CH2). As an initiator and accelerator, ammonium persulfate ($(NH_4)2S_2O_8$) and N, N, N′, N′-tetramethyl ethylenediamine ($C_6H_{16}N_2$) were utilized. Sodium dodecyl sulfate (SDS) ($CH_3(CH_2)_{11}OSO\ 3Na$) to reduce surface tension was utilized. Sigma-Aldrich provided all of the chemicals (Poole, UK).

Preparation of PAM\ZnO composite

In a 22:1 molar ratio, acrylamide (AM) and N, N′-methylene bisacrylamide (MBMA) monomers were used to make Sample 1. (AM: MBAM). The solution was then treated with 10 % (w/v) ammonium persulfate (APS) and 1 % (v/v) N,N,N′,N′-tetramethyl ethylenediamine (TEMED). A translucent gel was quickly formed by heating the fluid to 30 °C. Sample 2 was made by mixing zinc oxide with polyacrylamide, whereas sample 3 was made in an acidic environment. The 3 samples were dried for 3 h at 110 degrees Celsius.

Analytical techniques

Prepared samples were characterized using a Fourier Transform Infrared (FTIR) with a spectral range of 4,000 - 400 cm^{-1} as well as a resolution of 4 cm^{-1} spectrometer to study the intermolecular structure [19].

Homology modeling of UBE2C

As indicated in **Figure 1**, the sequence of UBE2C was obtained from UniProtKB. The template for modeling was discovered using the NCBI BLAST algorithm. The crystal structure of Human Mitotic-Specific Ubiquitin-Conjugating Enzyme (PDB code: 1I7K) with a resolution of 1.95 was identified as an acceptable template using NCBI BLAST against the PDB database. With an E-value of $1e^{-103}$, 99 percent of the residues in the template and target are identical.

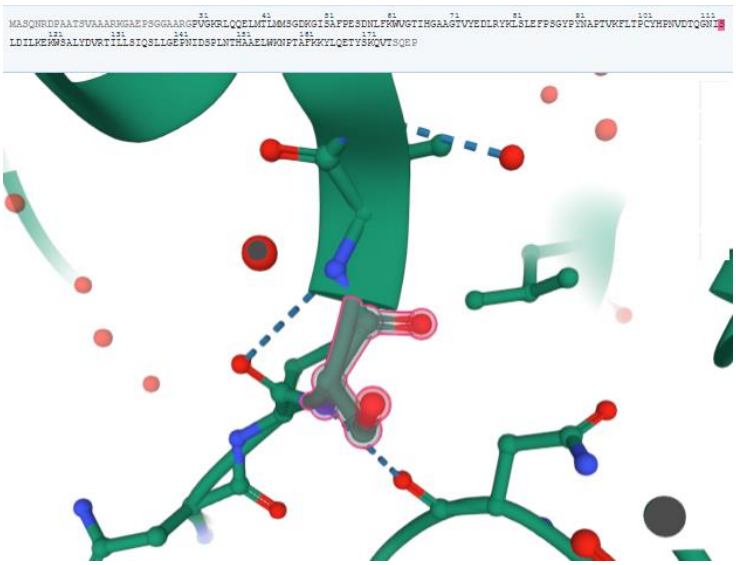

Figure 1 The crystal structure and the sequence of human mitotic-specific ubiquitin-conjugating enzyme with active site cysteine 114.

Calculation details

The Gaussian 09 program (Frisch 2010) performed all computations at Egypt's National Research Centre's spectroscopic department in Cairo (NRC). The density functional theory (DFT) approach optimized model molecules at Becke-3-parameters-Lee-Yang-Parrhybrid functional B3LYP using the basis set 6 - 31G. The bandgap energy is the difference between the highest occupied and lowest unoccupied molecular orbitals (HOMO/LUMO). Then, 2 physical parameters, TDM and binding energy, were computed for each structure analyzed. The molecular electrostatic potential (MESP) was estimated at the same level of theory for all structures studied in **Figures 7 - 11**.

Results and discussion

Part 1: Theoretical investigation

Building molecular modeling

Section 1 (The interaction probabilities between PAM and ZnO)

A model molecule was created to construct the polyacrylamide (PAM) polymer structure containing ZnO. In bladder cancer, the ubiquitin-conjugating enzyme 2C (UBE2C) mRNA and protein levels are abnormally elevated. A core catalytic domain exists in UBE2C (containing cysteine Cys114). PAM's model molecule is made up of acrylic units, as shown in **Figure 2**. **Figure 3** depicts the model molecule of zinc oxide (ZnO). **Figure 4** depicts the interaction of ZnO with PAM in 4 distinct places, each with 2 different bonds (covalent - Vanderwal), yielding 8 different probabilities for the interaction. Position 1 is shown in **Figures 4(a) - 4(b)**, where both covalent and Vanderwal interactions of ZnO occur through the carboxyl group at C_1. Position 2 is shown in **Figures 4(c) - 4(d)**, in which the contact occurs through the amide group (NH_2) of PAM at C_1 through both covalent and Vanderwal bonds. **Figures 4(e) - 4(f)** depict the interaction between ZnO and the (NH_2) group at C_3 of PAM through 2 bonds, covalent and Vanderwal, respectively. Finally, **Figures 4(g) - 4(h)** depict position 4, where covalent and Vanderwal bonds engage ZnO with the (NH_2) group at C_5 of PAM.

However, no covalent or Vanderwal bonds broke during the contact (C=O). At the same time, the interaction of ZnO with Polyacrylamide via a covalent bond (NH_2) required 1 hydrogen to be removed to complete the process.

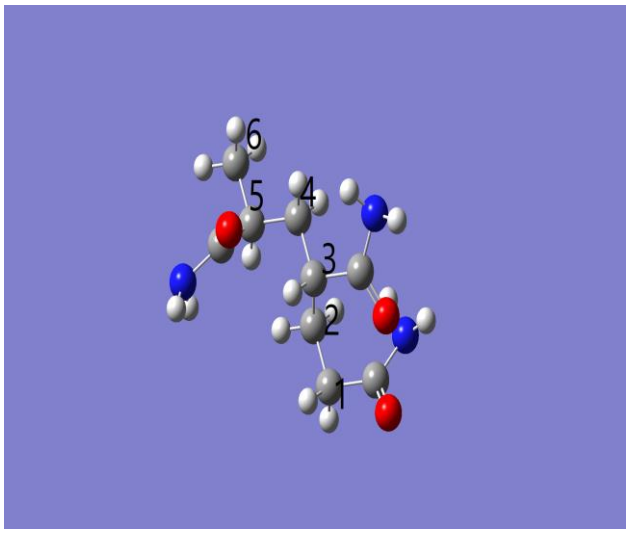

Figure 2 Represents a model molecule of polyacrylamide consisting of 6 units.

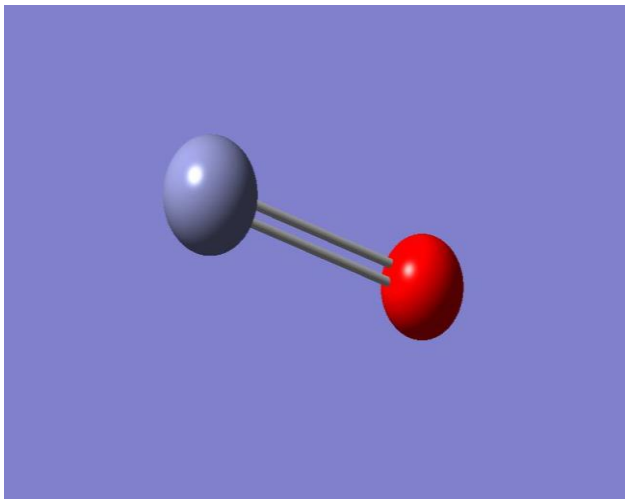

Figure 3 Shows the model molecule of zinc oxide ZnO.

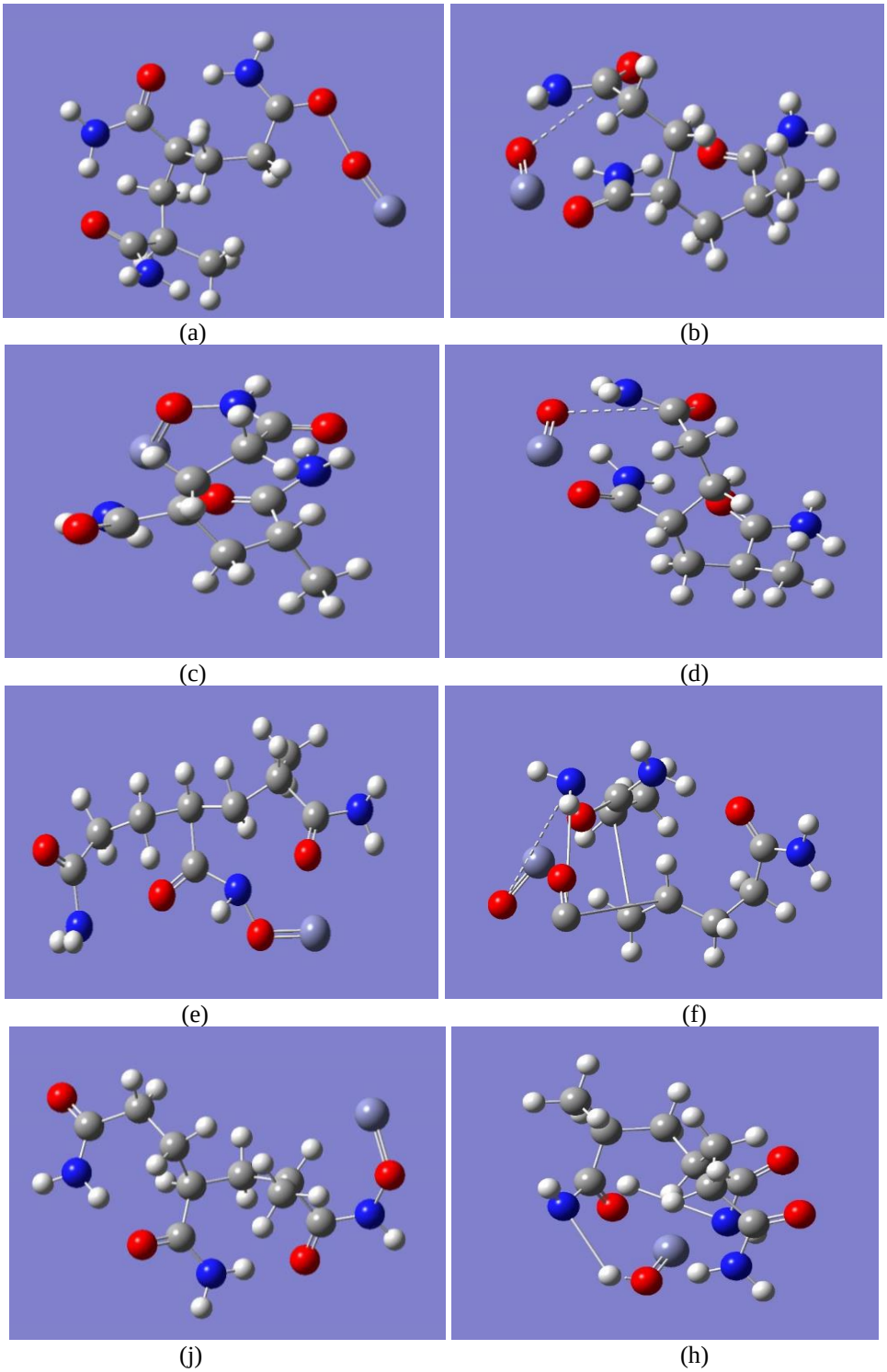

Figure 4 Represents the molecular model of (a), (b) position 1. The first covalent and vanderwal interaction of ZnO respectively proceed through the carboxyl group (C=O) of polyacrylamide at C_1. (c), (d) position 2, the second covalent and Vanderwal interaction of ZnO respectively proceed through the amide group (NH_2) of polyacrylamide at C_1. (e), (f) position 3, the third covalent and Vanderwal interaction of ZnO respectively proceed through the amide group (NH_2) of polyacrylamide at C_3. (j), (h) position 4, the 4 covalent and Vanderwal interaction of ZnO, respectively proceed through the amide group (NH_2) of polyacrylamide at C_5.

Section 2 (The interaction probabilities between PAM/ZnO nanocomposite and cysteine 114)

A model molecule was designed to build polyacrylamide PAM/ZnO with cysteine 114. Urine is an acidic medium that probability interaction more higher through Position 1 of the carboxyl group of C_1, which makes this probability higher. **Figure 5** shows the model molecule of Cystine 114. **Figure 6** shows the interaction of ZnO and PAM with Cys114 in the C_1 position by 2 different bonds (covalent - Vanderwal) in each position, giving 3 probabilities for the interaction. **Figures 6(a)** - **6(b)** represent the interaction proceeds through the ZnO linked with the carboxyl group of PAM at C_1 with the cystine amide group by Vanderwal and covalent interaction, respectively. At the same time, **Figure 6(c)** represents the interaction that proceeds through the O=Zn to the carboxyl group of PAM at C_1 with the cysteine amide group by covalent interaction.

There are no bonds that want to be fractured during the Vanderwal interaction. While the covalent interaction of ZnO with Polyacrylamide through (C=O) linked by the amide group of Cysteine 114 needs to remove 1 hydrogen to complete the process.

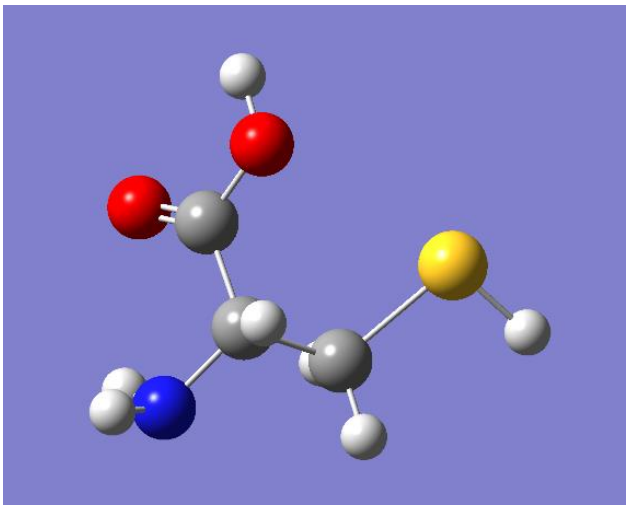

Figure 5 The model molecule of cysteine 114.

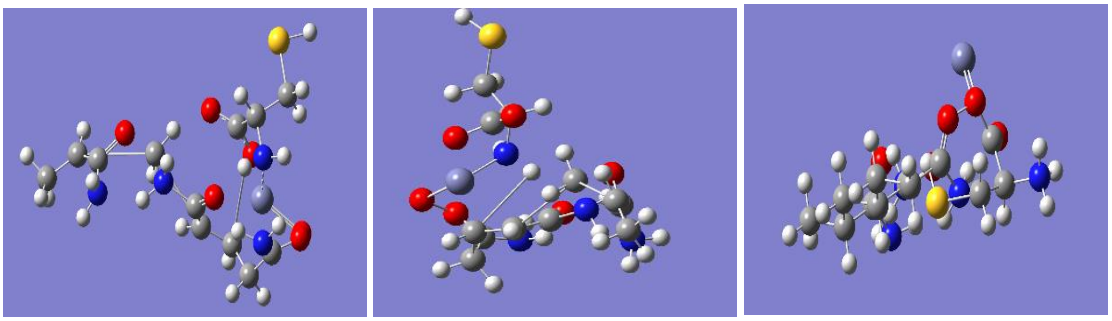

(a) (b) (c)

Figure 6 Represents the molecular model of Zinc oxide and the carboxyl group of polyacrylamide at C_1 with Cys114 (a) Vanderwal ZnO, (b) covalent ZnO, and (c) covalent OZn.

Total dipole moment TDM and bandgap energy ΔE

Two physical factors govern the reactive behavior of polyacrylamide structure and the interaction of PAM with ZnO: Total dipole moment TDM and E value. The reactivity increased when the overall dipole moment grew, and the energy gap shrank. The minimal E indicates that the material gets more conductive and promotes surface interactions. The bandgap is generally understood to indicate the amount of energy necessary to excite electrons from the highest occupied to the lowest empty molecular orbital. As a result, it represents how simple it is to have conductive material. As a result, bandgap energy can represent a substance's electrical activity.

Section 1 (for PAM/ZnO)

Table 1 represents the bandgap energy and TDM for different probabilities of the interaction between PAM and ZnO. **Tables 2** and **3** show the TDM and bandgap energy for the interaction between the NH_2 and C=O groups in C1, C3 and C5 of Polyacrylamide and ZnO metal oxide by Polyacrylamide and ZnO metal oxide, both covalent and Vanderwal bonds, respectively.

From **Tables 2** and **3**, it is evident that all 8 probabilities have a high reactivity because of their TDM above 5 deby. However, the PAM/ZnO (NH_2) covalent bond in C_1 and PAM/ZnO (NH_2) Vanderwal bond in C_3 represents the probability of highly electrical reactivity. Their calculated TDM has a max value between other probabilities and the min value for bandgap energy. While the interaction of PAM/ZnO (C=O) covalent and Vanderwal bond proceeded in C_1 depends on this position reflecting high electronegativity and giving a high electrical reactivity.

These 4-positions may be the most probable for interaction (covalent or Vanderwal) with Ubiquitin active sites (cys114)

Table 1 Shows the calculated energy gap ΔE, binding energy, and TDM for PAM\ZnO with different probabilities.

Structure		Dipole moment (debye)	Energy (eV)	Binding energy (eV)	Bandgap ΔE (eV)
Polyacrylamide		7.6245	6.8812×10^{11}		0.19896
ZnO		1.8900	1.7162×10^{12}		0.28055
Polyacrylamide-ZnO (C=O)	C_1 Covalent Position (1)	7.3249	2.4062×10^{12}	1.88×10^{9}	0.28302
	C_1 Weak Position (1)	10.9740	2.4063×10^{12}	1.98×10^{9}	0.22315
Polyacrylamide-ZnO (NH_2)	C_1 covalent Position (2)	7.7340	2.4057×10^{12}	1.38×10^{9}	0.02483
	C_1 Weak Position (2)	9.8068	2.4063×10^{12}	1.98×10^{9}	0.24364
	C_3 Covalent Position (3)	6.0566	2.3985×10^{12}	5.82×10^{9}	0.27227
	C_3 Weak Position (3)	12.3348	2.4061×10^{12}	1.78×10^{9}	0.19965
	C_5 Covalent Position (4)	5.4464	2.4057×10^{12}	1.38×10^{9}	0.02497
	C_5 Weak Position (4)	10.9953	2.4063×10^{12}	1.98×10^{9}	0.22305

Table 2 Show the total dipole moment of both covalent and Vanderwal bonds proceeded through amine and carboxyl group.

Structure		TDM (Debye)	
		Weak bond	Strong bond
Polyacrylamide-ZnO (C=O)	C_1	10.9740	7.3249
Polyacrylamide-ZnO (NH_2)	C_1	9.8068	7.7340
	C_3	12.3348	6.0566
	C_5	10.9953	5.4464

Table 3 Show the bandgap energy of both covalent and vanderwal bonds proceeded through amine and carboxyl group.

Structure		Bandgap energy (eV)	
		Weak bond	**Strong bond**
Polyacrylamide-ZnO (C=O)	C_1	0.22315	0.28302
Polyacrylamide-ZnO (NH_2)	C_1	0.24364	0.02483
	C_3	0.19965	0.27227
	C_5	0.22305	0.02497

Table 4 Represents the energy gap ΔE, binding energy, and TDM for different probabilities of the interaction between PAM and ZnO and cysteine 114.

Structure		Dipole moment (Debye)	Energy (eV)	Binding energy (eV)	Bandgap ΔE (eV)
Polyacrylamide		7.6245	6.8812×10^{11}		0.19896
ZnO		1.8900	1.7162×10^{12}		0.28055
Cysteine 114		0.8941	1.9542×10^{13}		0.23217
Polyacrylamide C=O -ZnO/ Cystine NH	C_1 Covalent	12.1503	8.9840×10^{13}	6.7853×10^{13}	0.06737
	C_1 Weak	12.1503	8.9840×10^{13}	6.7853×10^{13}	0.19401
Polyacrylamide C=O -OZn/ Cystine NH	C_1 Covalent	15.9651	8.7449×10^{13}	6.5502×10^{13}	0.19401

Section 2 (for PAM/ZnO/Cystine)

Urine is an acidic medium that stimulates the interaction through Position 1 of the carboxyl group of C_1, making this probability higher, blocking the interaction through the amide group of PAM. **Table 4** shows the calculated values of bandgap energy and binding energy, TDM of the interaction of the carboxyl group of PAM\ZnO with the amide group of cysteine.

The interrupted molecular electrostatic potential (MESP)

Only a yellow hue occurs in **Figures 7 - 14** indicating a uniform distribution of charges within and outside the surface with no change in electronegativity. As a result, studying the interaction of PAM with metal oxides is critical for manipulating its reactivity features.

This MESP contour illustrates the charge distributions for the examined PAM, PAM/ZnO, and PAM/ZnO/cysteine throughout the hues. The hues, as previously established, vary from negative to positive, continuing from red and yellow to blue. In other words, the rise in potential is described by the decreasing sequence red < orange < yellow < green < blue [19].

The MESP contour is a valuable tool for defining the surface of a particular structure since it specifies the places for electrophilic and nucleophilic reactions. In other words, the MESP might be highly useful in evaluating hydrogen bonding ability. This MESP contour illustrates the charge distributions for the examined PAM, PAM/ZnO and PAM/ZnO/cysteine throughout the hues. The hues, as previously indicated, run from negative to positive-going, from red and yellow to blue. In other words, the rise in potential is described by the decreasing order of red < orange < yellow < green < blue [20].

Section 1 (for PAM/ZnO)

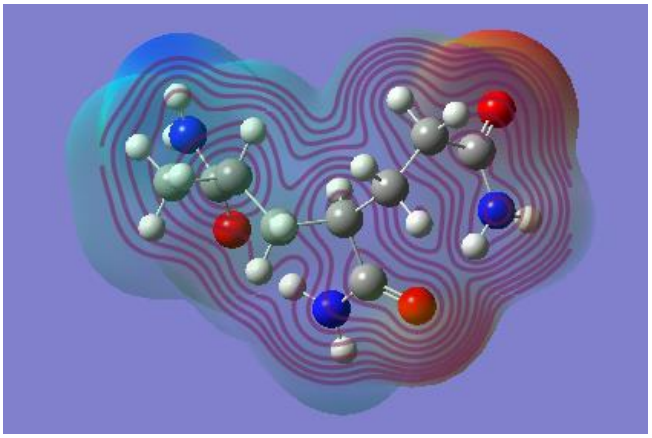

Figure 7 Represent the MESP of polyacrylamide.

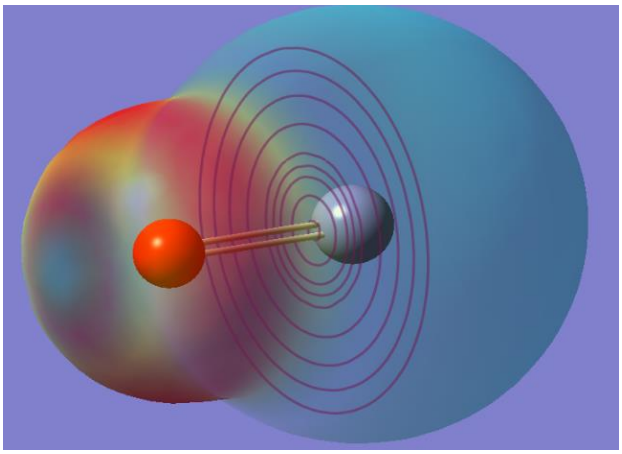

Figure 8 Represent the MESP of zinc oxide.

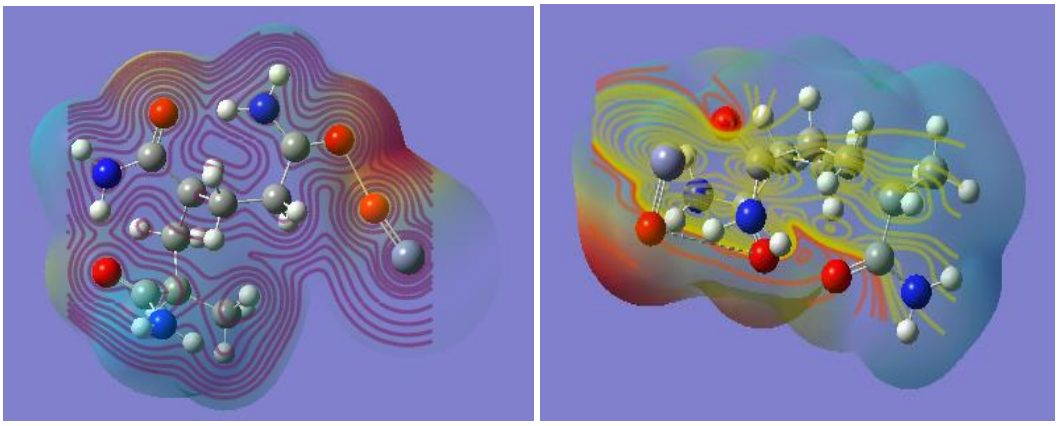

(a) (b)

Figure 9 Represents the MESP of (position 1), the interaction between ZnO and the carboxyl group of polyacrylamide at C_1 by (a) covalent and (b) vanderwal interaction.

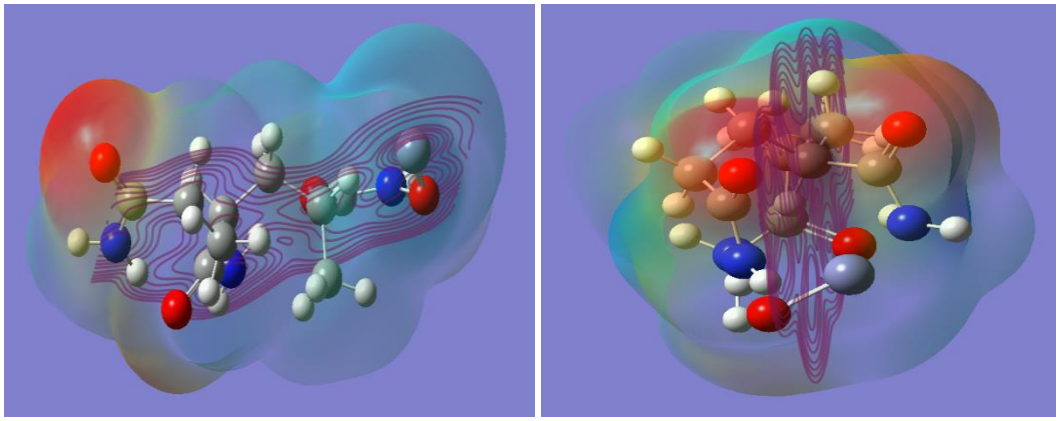

(c) (d)

Figure 10 Represents the MESP of (position 2) the interaction between ZnO and amide group of polyacrylamide at C_1 by (c) covalent and (d) vanderwal interaction.

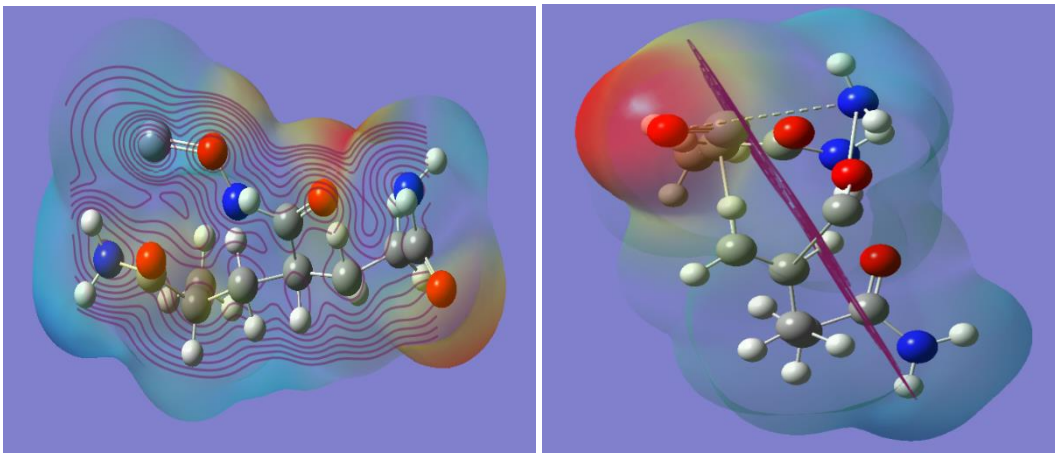

(e) (f)

Figure 11 Represents the MESP of (position 3) the interaction between ZnO and amide group of polyacrylamide at C_3 by (e) covalent and (f) vanderwal interaction.

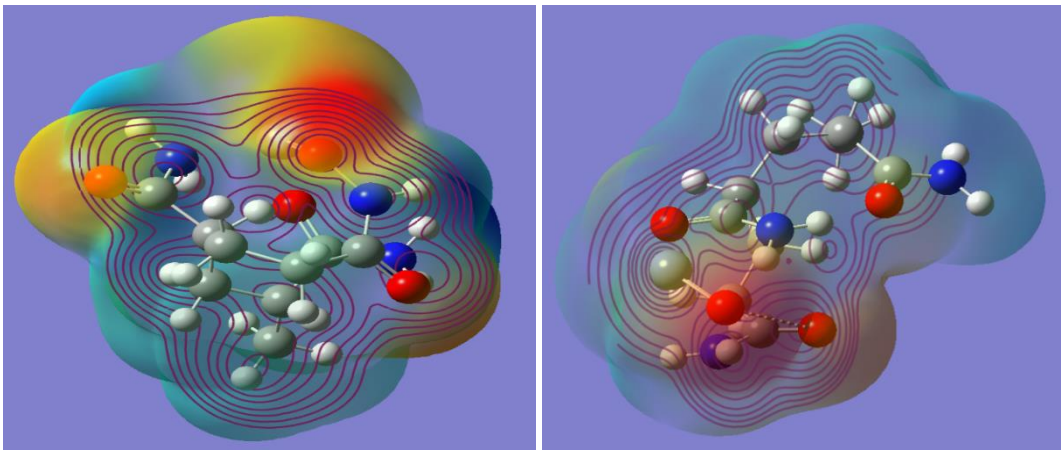

(j) (h)

Figure 12 Represents the MESP of (position 4) the interaction between ZnO and amide group of polyacrylamide at C_5 by (j) covalent and (h) vanderwal interaction.

Section 2 (for PAM/ZnO interaction with Cystine)

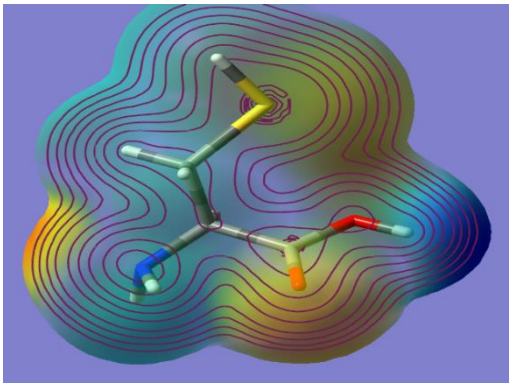

Figure 13 Represent the MESP of cysteine 114.

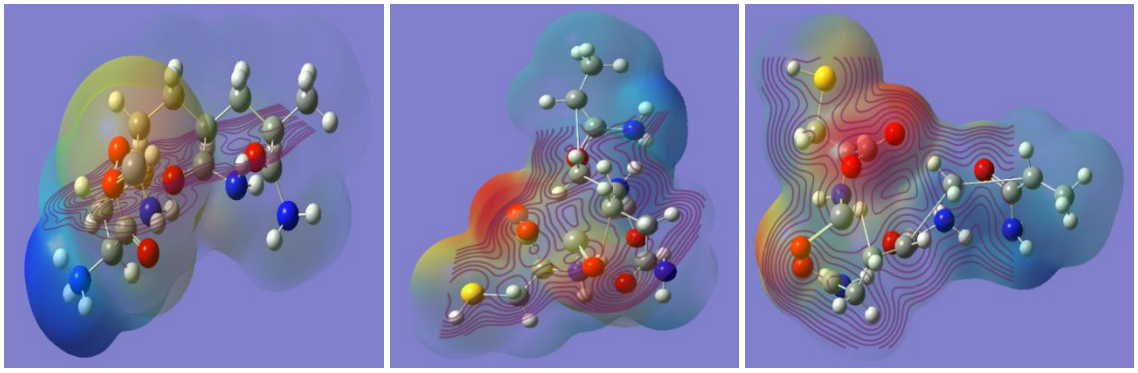

Figure 14 Represents the MESP of the interaction between zinc oxide and polyacrylamide (position 1) with cysteine 114 by (a) covalent ZnO, (b) Vanderwal ZnO, and (c) covalent OZn.

Part 2 experimental investigation

FTIR Characterization

As demonstrated in **Figure 15**, the bonding between ZnO and polyacrylamide was detailed using the FTIR approach [19]. The stretching vibrations of the hydrogen-bonded OH groups are responsible for the band at 3,000 cm^{-1} in the dry powder. The carbon Single bond hydrogen stretching vibration from organic molecules is connected to the absorption band at 2,935 cm^{-1}. The absorption band shows the existence of hydrogen-bonded OH at 2,100 cm^{-1}. Single bond COOH stretching vibrations are responsible for the features of the stretching bands between 1,450 and 1,660 cm^{-1}. Stretching vibrations of the CO^{-} anion cause the band at 1,321 cm^{-1}. The amide linkage is indexed to acrylamide in the 1,400 - 1,500 cm^{-1} range. However, bands caused by NO_3 stretch vibrations may be seen around 1,117 - 1,214 cm^{-1}. CH single bond OH is responsible for the absorption band at 1,042 cm^{-1}. Metal-oxygen bonding stretching vibrations are responsible for the 400 to 600 cm^{-1} range. The vibrational bands of ZnO are responsible for the lines seen at about 500, 540 and 664 cm^{-1}. Peaks in the 400 - 600 cm^{-1} range emerged due to the addition of ZnO to PAM. These peaks vanishes in acidic media.

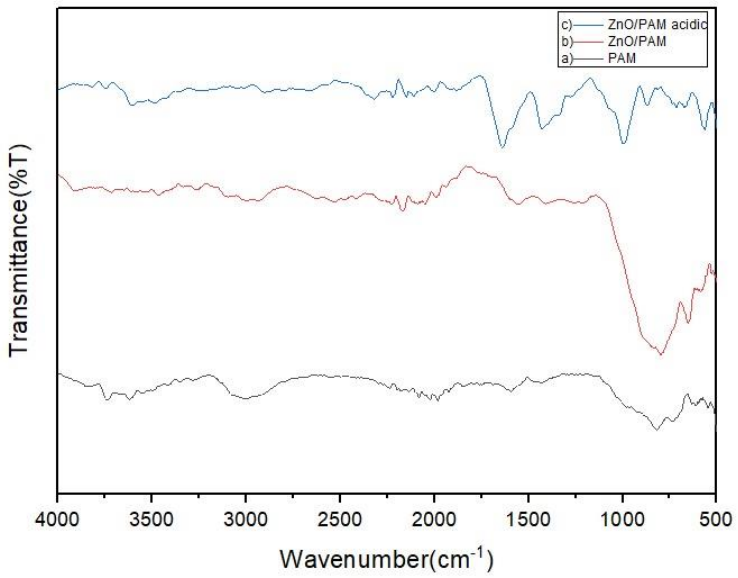

Figure 15 FTIR spectrum (a) PAM (b) PAM/ZnO (c) PAM/ZnO acidic.

Conclusions

A PAM\ZnO nanocomposite was synthesized and investigated using FTIR to ensure a good interaction. The disappearance of the 2 influential bands of ZnO in the spectrum confirmed the chemical interaction of PAM and ZnO in an acidic medium. This behavior makes covalent interaction more possible, giving varied electrostatic characteristics. Polyacrylamide PAM decorated with zinc oxide ZnO and cysteine 114 is subjected to DFT calculations at B3LYP/3-21g. The TDM, HOMO/LUMO bandgap energy, and MESP results could be utilized to guess the electrical properties. The present computational models could help estimate the reactivity and lead the research for optimizing biosensors, suggesting ideal composites for biosensors. The researched composite is a successful candidate for detecting phenomena, and it might operate as a biological sensor based on the studied theoretical and experimental data.

Acknowledgments

The authors extend their appreciation to Professor Medhat Ibrahim, Molecular Spectroscopy and Modeling Unit, Spectroscopy Department, National Research Centre, 33 El-Bohouth Str, Dokki, Giza 12622, Egypt.

References

[1] SJ Crabb and J Douglas. The latest treatment options for bladder cancer. *Br. Med. Bull.* 2018; **128**, 85-95.

[2] J Husband, J Olliff, MP Williams, C Heron and GR Cherryman. Bladder cancer: Staging with CT and MR imaging. *Radiology* 1989; **173**, 435-40.

[3] JJ Underwood, RS Quadri, SP Kalva, H Shah, AR Sanjeevaiah, MS Beg and PD Sutphin. Liquid biopsy for cancer: Review and implications for the radiologist. *Radiology* 2020; **294**, 5-17.

[4] J Marrugo-Ramírez, M Mir and J Samitier. Blood-based cancer biomarkers in liquid biopsy: A promising non-invasive alternative to tissue biopsy. *Int. J. Mol. Sci.* 2018; **19**, 2877.

[5] I Lodewijk, M Dueñas, C Rubio, E Munera-Maravilla, C Segovia, A Bernardini, A Teijeira, JM Paramio and C Suárez-Cabrera. Liquid biopsy biomarkers in bladder cancer: A current need for patient diagnosis and monitoring. *Int. J. Mol. Sci.* 2018; **19**, 2514.

[6] X Min, Y Zhuang, Z Zhang, Y Jia, A Hakeem, F Zheng, Y Cheng, BZ Tang, X Lou and F Xia. Lab in a tube: Sensitive detection of MicroRNAs in urine samples from bladder cancer patients using a single-label DNA probe with AIEgens. *ACS Appl. Mater. Interfac.* 2015; **7**, 16813-8.

[7] XM Piao, EJ Cha, SJ Yun and WJ Kim. Role of exosomal miRNA in bladder cancer: A promising liquid biopsy biomarker. *Int. J. Mol. Sci.* 2021; **22**, 1713.

[8] AI Nossier, S Eissa, MF Ismail, MA Hamdy and HMES Azzazy. Direct detection of hyaluronidase in urine using cationic gold nanoparticles: A potential diagnostic test for bladder cancer. *Biosens. Bioelectron.* 2014; **54**, 7-14.
[9] S Eissa, SM Shawky, M Matboli, S Mohamed and HM Azzazy. Direct detection of unamplified hepatoma upregulated protein RNA in urine using gold nanoparticles for bladder cancer diagnosis. *Clin. Biochem.* 2014; **47**, 104-10.
[10] Y Xu, C Luo, J Wang, L Chen, J Chen, T Chen and Q Zeng. Application of nanotechnology in the diagnosis and treatment of bladder cancer. *J. Nanobiotechnol.* 2021; **19**, 393.
[11] SK Patel, J Parmar, V Sorathiya, TK Nguyen and V Dhasarathan. Tunable infrared metamaterial-based biosensor for detection of hemoglobin and urine using phase change material. *Sci. Rep.* 2021; **11**, 7101.
[12] JW Rasmussen, E Martinez, P Louka and DG Wingett. Zinc oxide nanoparticles for selective destruction of tumor cells and potential for drug delivery applications. *Expet. Opin. Drug Deliv.* 2010; **7**, 1063-77.
[13] HFE Sharif, F Giosia and SM Reddy. Investigation of polyacrylamide hydrogel-based molecularly imprinted polymers using protein gel electrophoresis. *J. Mol. Recogn.* 2022; **35**, e2942.
[14] M Ogiso, N Minoura, T Shinbo and T Shimizu. DNA detection system using molecularly imprinted polymer as the gel matrix in electrophoresis. *Biosens. Bioelectron.* 2007; **22**, 1974-81.
[15] G Selvolini and G Marrazza. MIP-based sensors: Promising new tools for cancer biomarker determination. *Sensors* 2017; **17**, 718.
[16] Y Wang, M Hana, G Liu, X Hou, Y Huang, K Wu and C Li. Molecularly imprinted electrochemical sensing interface based on in-situ-polymerization of amino-functionalized ionic liquid for specific recognition of bovine serum albumin. *Biosens. Bioelectron.* 2015; **74**, 792-8.
[17] CP Chou, NC Huang, SJ Jhuang, HB Pan, NJ Peng, JT Cheng, CF Chen, JJ Chen and TH Chang. Ubiquitin-conjugating enzyme UBE2C is highly expressed in breast microcalcification lesions. *PLoS One* 2014; **9**, e93934.
[18] A Mbeutcha, I Lucca, R Mathieu, Y Lotan and SF Shariat. Current status of urinary biomarkers for detection and surveillance of bladder cancer. *Urol. Clin.* 2016; **43**, 47-62.
[19] A Aftab, A Ismail, S Khokhar and ZH Ibupoto. Novel zinc oxide nanoparticles deposited acrylamide composite used for enhancing the performance of water-based drilling fluids at elevated temperature conditions. *J. Petrol. Sci. Eng.* 2016; **146**, 1142-57.
[20] H Elhaes, M Morsy, I Yahia and M Ibrahim. Molecular modeling analyses for electronic properties of CNT/TiO2 nanocomposites. *Opt. Quant. Electron.* 2021; **53**, 269.